HHS Public Access

Author manuscript

Mol Cancer Res. Author manuscript; available in PMC 2022 May 01.

Published in final edited form as:

Mol Cancer Res. 2021 November ; 19(11): 1917–1928. doi:10.1158/1541-7786.MCR-20-0753.

Gene body methylation of the lymphocyte-specific gene *CARD11* results in its overexpression and regulates cancer mTOR signaling

Michael H. McGuire[#1], **Santosh K. Dasari**[#1], **Hui Yao**[2], **Yunfei Wen**[1], **Lingegowda S. Mangala**[1], **Emine Bayraktar**[1], **Wencai Ma**[2], **Cristina Ivan**[5], **Einav Shoshan**[3], **Sherry Y. Wu**[1], **Eric Jonasch**[4], **Menashe Bar-Eli**[3], **Jing Wang**[2], **Keith A. Baggerly**[2], **Anil K. Sood**[1,3,5,6,*]

[1]Department of Gynecologic Oncology and Reproductive Medicine, The University of Texas MD Anderson Cancer Center, Houston, TX 77030, USA

[2]Department of Bioinformatics and Computational Biology, The University of Texas MD Anderson Cancer Center, Houston, TX 77030, USA

[3]Department of Cancer Biology, The University of Texas MD Anderson Cancer Center, Houston, TX 77030, USA

[4]Department of Genitourinary Medical Oncology, The University of Texas MD Anderson Cancer Center, Houston, TX 77030, USA

[5]Department of Experimental Therapeutics, The University of Texas MD Anderson Cancer Center, Houston, TX 77030, USA

[6]Department of Center for RNA Interference and Non-Coding RNA, The University of Texas MD Anderson Cancer Center, Houston, TX 77030, USA

[#] These authors contributed equally to this work.

Abstract

Investigations into the function of non-promoter DNA methylation have yielded new insights into epigenetic regulation of gene expression. Previous studies have highlighted the importance

[*]Correspondence: Anil K. Sood: (713) 404-8831, asood@mdanderson.org, Department of Gynecologic Oncology, Unit 1362, The University of Texas MD Anderson Cancer Center, 1155 Herman Pressler, Houston, TX 77030.

AUTHOR CONTRIBUTIONS

MH McGuire: Conceptualization, data curation, formal analysis, investigation, validation, visualization, methodology, and writing—original draft, review and editing. **SK Dasari:** Conceptualization, data curation, formal analysis, investigation, validation, visualization, methodology, and writing—original draft, review and editing. **H Yao:** Data curation, formal analysis, investigation, validation, methodology and visualization. **Y Wen:** Data curation, formal analysis, investigation, validation, and visualization. **LS Mangala:** Methodology and investigation. **E Bayraktar:** Methodology and investigation. **Wencai Ma:** Data curation, formal analysis, investigation, validation and methodology. **Cristina Ivan:** Data curation, formal analysis. **E Shoshan:** Formal analysis, validation, and investigation. **SY Wu:** Validation, visualization, and methodology. **E Jonasch:** Conceptualization, methodology, resources, and supervision. **M Bar-Eli:** Conceptualization, methodology, resources, and supervision. **Jing Wang:** Conceptualization, methodology, resources, and supervision. **KA Baggerly:** Conceptualization, resources, data curation, formal analysis, supervision, funding acquisition, validation, investigation, visualization, methodology, and project administration. **AK Sood:** Conceptualization, resources, data curation, formal analysis, supervision, funding acquisition, validation, investigation, visualization, methodology, project administration, and writing—original draft, review, and editing.

Conflict of interests:

Anil K. Sood announces the following relationships: consulting (Kiyatec, Merck, Astra Zeneca); stock holder (BioPath); research funding (M-Trap). All other authors have no financial relationships to report.

of distinguishing between DNA methylation in discrete functional regions; however, integrated non-promoter DNA methylation and gene expression analyses across a wide number of tumor types and corresponding normal tissues have not been performed. Through integrated analysis of gene expression and DNA methylation profiles, we examined 32 tumor types and identified 57 tumor suppressors and oncogenes out of 260 genes exhibiting a correlation of > 0.5 between gene body methylation and gene expression in at least 1 tumor type. The lymphocyte-specific gene CARD11 exhibits robust association between gene body methylation and expression across 19 of 32 tumor types examined. It is significantly overexpressed in kidney renal cell carcinoma (KIRC) and lung adenocarcinoma (LUAD) tumor tissues in comparison to respective control samples; and is significantly associated with lower overall survival in KIRC. Contrary to its canonical function in lymphocyte NF-kB activation, CARD11 activates the mTOR pathway in KIRC and LUAD, resulting in suppressed autophagy. Furthermore, demethylation of a CpG island within the gene body of CARD11 decreases gene expression. Collectively, our study highlights how DNA methylation outside the promoter region can impact tumor progression.

Keywords

gene body methylation; CARD11; epigenetics; cancer

INTRODUCTION

Methylation is the most common DNA modification in the genome and plays an important role in regulating gene expression (1). This process is a critical means by which cells containing the same DNA template can differentiate into a spectacular array of different cell types (2). The most studied type of DNA methylation is that which occurs on CpG islands within a gene's promoter region (3). This has been shown to powerfully repress transcription through multiple mechanisms, particularly through inducing formation of heterochromatin by recruiting histone modifiers (4). However, promoter DNA methylation only accounts for a small fraction of genomic methylation (5). Recent studies have begun to unravel the impact of DNA methylation outside of the promoter region (6–9). Enhancer (10, 11), gene body (12, 13), and intergenic (14) DNA methylation have all been implicated in various forms of gene regulation (15). Despite these recent advancements, much remains to be understood about region-specific DNA methylation.

Because DNA methylation is essential for numerous cellular functions, aberrant DNA methylation is frequently observed in a large variety of unrelated diseases (16–18). This phenomenon has been implicated in conditions such as neurodegenerative disorders (19–21), cardiovascular (22–24), autoimmune (25–27), and many other diseases. Most prominently, aberrant DNA methylation is closely tied to cancer pathogenesis (28). Since cancer involves a fundamental alteration of a cell's developmental state, global changes to DNA methylation are ubiquitously observed across nearly every type of cancer. These changes are involved in early phases of tumorigenesis through cellular de-differentiation, suppression of tumor suppressor genes, and enhanced expression or reduced repression of oncogenes (29). Furthermore, changes to the DNA methylome have been causally linked

to metastasis (30), emergence/maintenance of chemoresistance (31), and alterations to the tumor microenvironment (32).

Considering the immense involvement of this epigenetic modification on cancer formation and progression, investigating how aberrant DNA methylation occurs is crucial for designing novel therapeutic approaches. In particular, gene body methylation has emerged as a contributor to cancer pathogenesis (33, 34). CpG sites in promoter or enhancer regions are often hypermethylated and packed into heterochromatin, thereby decreasing access to transcription activators and leading to transcriptional repression (35). In addition, recent reports, including studies from our laboratory, have shown that hypermethylation of CpG sites located in gene body region lead to increased gene expression (33, 36). Contrary to promoter DNA methylation, this modification has been shown to affect gene expression by multiple mechanisms, depending on the specific locus and context. For example, DNMT3B-mediated gene body methylation, especially within myc-regulated genes, has been demonstrated to activate oncogenes in colorectal cancer (33). Despite these recent advances, mechanisms by which gene body methylation is intertwined in cancer pathogenesis is not well understood.

In the work presented here, we examined the relationship between gene body DNA methylation and gene expression across a group of oncogenes and tumor suppressors well-known to be involved in tumorigenesis and tumor progression. Through this analysis, we uncovered a robust positive correlation between *CARD11* gene body DNA methylation and gene expression. Collectively, our results reveal how specific gene body methylation can induce aberrant expression of a gene that promotes cancer pathogenesis through a non-canonical pathway.

MATERIALS AND METHODS

Study design

Sample size: We used all available tumor and normal tissue samples in the TCGA database, which includes data on about 11,000 US cancer patients. There are no publication restrictions on these data according to the TCGA data policy (http://cancergenome.nih.gov/publications/publicationguidelines). Rules for stopping data collection: N/A. Data inclusion and exclusion criteria: correlation coefficient cutoff was set at 0.5. Outliers: No outliers were excluded from this analysis. Selection of endpoints: N/A.

TCGA tissue selection

For this analysis, we used tumor and normal tissue samples from 32 tumor types. Illumina HiSeq RNASeqV2 and Illumina Human Methylation 450 k data were available at the time of our initial download on March 26, 2013. The corresponding clinical data of KIRC used for the survival analysis were downloaded from the TCGA data portal and were current as of January 8, 2014.

Methylation and gene expression data

We used the level-3 log2-transformed RNASeqV2 data of the TCGA cohort to analyze gene expression. To avoid errors for RNASeq raw counts of 0, all values were offset by 1 prior to obtaining logs. We used level-3 beta values of the Illumina Human Methylation 450 K array data of the TCGA cohort to analyze gene methylation. The TCGA data was obtained through TCGAGeneReport package (version: 2015-12-09-0638, https://github.com/GeneSurvey/TCGAGeneReport/). The datasets generated or analyzed during the current study are available in the TCGA database repository, https://cancergenome.nih.gov/ and https://github.com/MD-Anderson-Bioinformatics/GeneSurvey.

Gene methylation and expression correlation

All analyses were performed using R software, version 2.15.1. Using the complete set of probes targeting CpG dinucleotides, we explored the relationship between the proportion of methylation in gene body and the corresponding log-transformed gene expression. We used the Spearman rank statistic to quantify the correlation for each pair. Because we expected these patterns to vary by the tissue source site, we calculated coefficients individually for all tissue types for which we had data from both the 450 k methylation and RNASeq arrays. In addition, we used CIBERSORT analytical tool (CIBERSORT, RRID:SCR_016955) to estimate the abundance of lymphocyte cell populations in LUAD and KIRC TCGA cohorts using normalized RNASeq data. Eventually, we calculated the Spearman correlation coefficients between *CARD11* expression levels and estimated abundances of immune and other cell types.

Gene Set Enrichment Analysis

Gene Set Enrichment Analysis (GSEA v2.0) was used to analyze the association between CARD11 expression and various biological pathways; we used pre-defined gene sets from the Molecular Signatures Database, MSigDB (Gene Set Enrichment Analysis, RRID:SCR_003199). Samples from the TCGA datasets were divided into high- or low-*CARD11* expression groups using the median value as the cutoff. Default settings were used and False Discovery Rate (FDR) was calculated. A gene set is considered significantly enriched when the FDR score is less than 0.25.

Cell Culture

UOK111 (RRID:CVCL_B090), Caki (RRID:CVCL_0234) and A498 (RRID:CVCL_1056) renal cell carcinoma cells were a kind gift from Dr. Eric Jonasch. These cells were grown in DMEM (Clontech) + 10% FBS (Thermo Fisher Scientific) + 1% PenStrep (Thermo Fisher Scientific), and were split upon reaching 80% confluence. H1975 (RRID:CVCL_1511) lung adenocarcinoma cells were a kind gift from Dr. John Heymach. These were grown using RPMI (Clontech) + 10% FBS (Thermo Fisher Scientific) + 0.1% gentamycin (Thermo Fisher Scientific). These cells were split upon reaching 80% confluence. Each cell line was validated using STR testing and mycoplasma detection PCR analysis.

Western Blotting

Cell pellets were re-suspended in RIPA buffer and quantified using the BCA assay (Thermo Scientific Pierce BCA Protein Assay Kit). Equal amounts of protein were run on an SDS-PAGE gel (8%−12%), then transferred to a nitrocellulose membrane and incubated in 5% milk in TBS-T for one hour, followed by incubation in primary antibodies overnight. Blots were then washed with TBS-T three times for 20 minutes each, then incubated in HRP conjugated secondary antibodies (GE Healthcare, 1:2000) for one hour. HRP was visualized using an enhanced chemiluminescence detection kit (PerkinElmer). The following antibodies were used: anti-CARD11 (Cell Signaling Technology Cat# 4435, RRID:AB_2070359; Abcam Cat# ab113409, RRID:AB_10861854; 1:1000), anti-phospho S6 (Cell Signaling Technology Cat# 2215, RRID:AB_331682; 1:1000), anti-S6 (Cell Signaling Technology Cat# 2217, RRID:AB_331355; 1:3000), anti-GAPDH (Sigma-Aldrich Cat# G8795, RRID:AB_1078991: 1:5000), anti-LC3B (Cell Signaling Technology Cat# 2775, RRID:AB_915950; 1:1000), anti-Alpha Tubulin (Sigma-Aldrich Cat# T9026, RRID:AB_477593; 1:3000) and anti-Beta Actin (Sigma-Aldrich Cat# A1978, RRID:AB_476692; 1:3000).

SiRNA Transfection

Cells to be transfected were plated in 6-well plates at 50% confluence on the day of transfection. For each well, 1.3μg of siRNA was added to 50μL of serum-free media, and in a separate tube 4μL of FuGene HD Transfection Reagent (Promega) was incubated in 50 μL of serum-free media for 5 minutes. The siRNA/media mixture was then added dropwise to the transfection reagent mixture, mixed, then incubated for 15 minutes. The siRNA mixture was added dropwise to each well, and after 4-6 hours serum-free media was replaced with complete media. Reverse transfections were performed 2-3 days after forward transfections. 4μg of siRNA per well was added to 500 μL serum-free media. In a separate tube, 8μL of RNAiMAX (Thermo Fisher Scientific) was added to 500 μL of serum-free media and incubated for 5 minutes. The siRNA mixture was then added dropwise into the RNAiMAX mixture. Cells were then lifted, suspended in 5% FBS media, and counted. 400,000 cells in 2 mL media per well were then added on top of the siRNA mixture. 4-6 hours later, the media was removed and complete media was added.

Virus production and transduction

To produce virus for transduction, HEK293T (RRID:CVCL_0063) cells were plated in 10 cm plates at 1.5×10^6 cells per plate. The next day, 5 μg of ptfLC3 (LC3 fused to a EGFP+RFP tag) or pLVX-TetOne-CARD11-Puro lentiviral plasmid (Epoch Life Sciences) was combined with 2.5 μg of the pMD2.G (RRID:Addgene_12259) envelope plasmid and 2.5 μg of the psPAX2 (RRID:Addgene_35002) packaging plasmid, into 250 μL of DMEM SFM, per 10 cm plate. Separately, 30 μL of Lipofectamine 2000 (Thermo Fisher Scientific) was incubated in 250 μL DMEM SFM. After 5 minutes, the lentiviral combination was pipetted into the Lipofectamine solution dropwise. This mixture was then incubated for 20 minutes, then added dropwise onto the HEK293T cells. After 4 hours, the media was changed to 10 mL DMEM + 15% FBS + 0.1% gentamycin. After 3 days, the media was harvested and passed through a 0.45 μm filter, then added to the cell type that would be

transduced. Two days later, the media was changed to that which matches the transduced cell type.

SiRNAs, gRNAs and primers

For RNA and DNA sequences please see attached supplementary table 1. *CARD11*-NAT sequences were designed specifically to target the exon of *CARD11*-NAT while not targeting the exon of *CARD11.*

Cellular Function Assays

For both cell lines, cells were subject to an initial siRNA transfection at 50% confluence in a 6-well plate, followed by a reverse transfection using 400,000 cells 3 days later. Two days after the reverse transfection, cells were harvested for analysis. For the proliferation assay, Click-iT EdU Alexa Fluor 488 assay (Thermo Fisher Scientific) was employed. Cells were incubated with 10μM EdU for 1 hour, then fixed using 3.7% formaldehyde and permeabilized using 0.5% Triton X-100. Alexa Fluor-488 was then added and flow cytometry was performed on cells to quantify the percent of cells that stained positive for EdU-Alexa Fluor-488 as a readout for proliferation. For cell cycle assay, the same batch of cells used for the proliferation assay was incubated in DAPI for 5 minutes, then flow cytometry for DAPI staining was used to quantify the stages of cell cycle for each cell population. The apoptosis assay was performed using the FITC Annexin V Apoptosis Detection Kit I (BD Biosciences). After being stained with FITC and Annexin V, cells were sorted based on staining to quantify percent of population in early and late stage apoptosis.

Quantitative Reverse Transcriptase PCR

RNA was extracted from cells using the Direct-zol RNA isolation kit (Zymo). Briefly, cells were washed with PBS, then re-suspended in TRIzol (Thermo Fisher Scientific), then run through a column, as instructed by the Direct-zol protocol. RNA was quantified using NanoDrop, then 500ng of RNA was used as a template for cDNA synthesis using the Verso cDNA synthesis kit (Thermo Fisher Scientific). 25ng of cDNA was then used for qPCR analysis. Briefly, in each well, 1μL each of 100μM primers was added to 25ng cDNA and 5μL SYBR Green PCR Master Mix (Thermo Fisher Scientific). This mixture was then placed in the RT-PCR machine (Applied Biosystems), and the following program was undertaken: 50°C 2 minutes, 95°C 10 minutes, (95°C 15 seconds, 60°C 1 minutes) x 40 cycles. The Ct values were then compared and the ΔΔCt was calculated. This was then used to quantify the relative changes in mRNA expression across samples.

Autophagy Assay

Cells were first transfected with siRNA and then subjected to reverse transfection, as outlined above. Two days after reverse transfection, 200 nM bafilomycin A1 (Sigma Aldrich) was added to complete media. Cells were incubated with bafilomycin A1-containing media for 4 hours, then protein was harvested and run on an SDS-PAGE gel as outlined above.

Live Cell Microscopy

To measure differences in autophagic flux after knockdown of *CARD11*, 100,000 UOK111 cells expressing GFP/RFP-tagged LC3 were transfected with *CARD11* siRNA as listed above, then reverse transfected and plated on a 2-well chamber slide. One day later, cells were imaged using confocal fluorescent microscopy. Eight spots for control and treatment group that were similar in number of cells and fluorescent intensity were selected for imaging. Real-time imaging was performed for 55h with 15-minute intervals, and imaged with Nikon A1R MP+ multiphoton confocal microscope. Levels of late-stage autophagy were quantified by contrast of GFP-LC3 versus RFP-LC3 fluorescence signal levels. The fluorescence intensities were quantified using ImageJ (ImageJ, RRID:SCR_003070) for the ratio of RFP/GFP expression within the cells.

DNA Methylation Analysis by PCR

Cells undergoing methylation analysis had their whole genome DNA isolated using the DNeasy Blood & Tissue kits. 500ng of DNA was then subjected to bisulfite treatment using the EZ DNA Methylation-Direct Kit (Zymo). PCR was then performed on the bisulfite-treated DNA using the method described above. In order to discern between methylated and unmethylated CpG dinucleotides, primers for each CpG was designed with their 3’ end falling on the CpG of interest. The primers probing for unmethylated CpG had the 3’ end of their sequence be complementary to TpG, whereas the primers probing for methylated CpG were complementary to CpG, because after bisulfite treatment, all unmethylated CpGs become TpGs. The ΔΔCt of the PCR for each primer were then compared to determine relative levels of methylation in the cell population.

Methylation analysis

One microgram of genomic DNA was treated with sodium bisulfite using the EZ DNA Methylation-Gold Kit (Zymo Research, Irvine, CA) according to the manufacturer’s protocol. The samples were eluted using 40 μl of M-Elution Buffer, then 2μl of the eluted product were subjected to PCR analysis. The pyrosequencing analysis as well as the bisulfite conversion were carried out at the DNA Methylation Analysis Core, UT MD Anderson Cancer Center.

The Pyromark Assay Design SW 1.0 (Qiagen) software was used for design of the *CARD11* primers. These primers were designed using the following parameters: approximately 5bp away from the CpG to be analyzed, a primer with an annealing temperature of within 5°C of 40°C was designed for sequencing. Next, two primers representing the forward and the reverse flanking the sequencing primer were created. To determine the best annealing temperature, gradient PCR was performed. The total combined volume of 20μL was employed for a single reaction, as described (37). Streptavidin-sepharose high-performance beads (GE Healthcare Life Sciences) were used in purification of the PCR product. The biotinylated products of the PCR reaction and primer used for sequencing (3.6 pmol per reaction) were then co-denatured using the guide for sample preparation. The sequencing was then carried out using a PyroMark Q96 ID instrument. The reagents used for this reaction are the Pyromark Gold Q96 variety (Qiagen). The PyroMark Q96 software was

used to determine the amount of methylation for each analyzed CpG. In each sample, the methylation average, as well as the duplicates, were recorded.

Antisense Overexpression Constructs

To overexpress the *CARD11* natural antisense transcript, the cDNA of the spliced transcript was synthesized and inserted into the pMX vector by GeneArt protocol (Thermo Fisher Scientific). This plasmid was amplified in DH5α competent E. coli (Thermo Fisher Scientific) by adding 50 ng into 50 μL bacteria, incubating on ice for 30 minutes, at 42°C for 45 seconds, and then on ice for 2 minutes. 50 μL of LB broth (Thermo Fisher Scientific) was then added and cells were incubated for 1 hour at 37°C. Cells were then spread on an LB-agar plate containing ampicillin. The plate was then incubated overnight, and colonies were picked the next morning. Colonies were grown in 3 mL of LB broth for 8 hours, then transferred to 50 mL of LB broth for 6 hours. Cells were then spun at 4,000xg for 15 minutes at 4°C, then the plasmids were isolated from the cell pellet using the QIAGEN midiprep kit. Plasmids were suspended in 50 μL water, then quantified using NanoDrop (Thermo Fisher Scientific). 500 ng of plasmid was digested with 2μL of EcoRI (Thermo Fisher Scientific) for 45 minutes. The digested product was run on a 1% agarose gel, and the band matching the size of the *CARD11*-NAT cDNA sequence was cut out and isolated using the QIAquick Gel Extraction Kit (Qiagen). Additionally, 500 ng of the PCRII expression vector was cut with EcoRI, run on a gel, and isolated as described above. The cut PCRII vector and *CARD11*-NAT cDNA were then added together with 1 μL T4 DNA ligase for 1 hour at 37°C, then transformed into DH5α cells as described above in order to obtain a PCRII construct with *CARD11*-NAT cDNA inserted within.

Cas9-Tet1 fusion construct

The nickase-dead dCas9-VP64-T2A-GFP plasmid was ordered from Addgene (RRID:Addgene_61422). The VP64 was replaced by the TET1 catalytic domain using the following primers:

hTet1_CD_BamHI_F: ATTAGGATCCCTGCCCACCTGCAGCTGTCTT

hTet1_CD_NheI_R: ATTAGCTAGCGACCCAATGGTTATAGGGCCCC

The PCR product was amplified using DNA isolated from HT-29 (RRID:CVCL_0320) colorectal cells using the method described above, as these cells contain high *TET1* expression. The program consisted of 95°C for 2m → (95°C for 15s → 60°C for 15s → 68°C for 45s) x 30 cycles → 68°C for 5m. This product as well as the dCas9 plasmid (RRID:Addgene_61422) were cut using BamHI and NheI (Fermentas). Both were run on a 1% agarose gel, and the bands were isolated using a gel purification kit (Qiagen). The products were then incubated together with T4 ligase (NEB) at a 1:3 vector to insert ratio. This was then transformed into competent *E.coli* and plasmids were checked for proper insertion using the restriction digestion method described above. Once confirmed, viruses were prepared from this plasmid using the method described above. H1975 cells were transduced and after 7 days, cells were sorted using flow cytometry for GFP expression and later confirmed by western blot analysis.. Short guiding RNAs against the region of interest were selected using the Broad Institute CRISPRko design tool. These sgRNAs were cloned

using the SAM target sgRNA cloning protocol. Site-specific methylation was evaluated using the DNA methylation direct kit as described above.

Doxycycline-inducible stable cell generation

Dox-inducible CARD11 expressing A498 cells were generated using lentiviral pLVX-TetOne-CARD11-Puro plasmid (Epoch Life Sciences). Cells were grown in six-well dishes and infected with lentiviruses at a high multiplicity of infection. The following day the cells were trypsinized and transferred to a T75 flask and were further selected with puromycin.

Mouse xenograft renal cancer model

Female athymic NCr-nude mice (IMSR Cat# TAC:ncrnu, RRID:IMSR_TAC:ncrnu) were obtained from Taconic Biosciences (Rensselaer, NY). Animals were cared for according to guidelines set forth by the Association for Assessment and Accreditation of Laboratory Animal Care and by the US Public Health Service policy on Humane Care and Use of Laboratory Animals. All mouse studies were approved and supervised by the Institutional Animal Care and Use Committee (IACUC) at the MD Anderson Cancer Center. 8-12 weeks old female mice (at the time of injection) were used for the experiments. To establish the overexpression tumor model, we injected doxycycline-inducible CARD11 expressing A498 cells (10 million cells/mouse in 150 μL of HBSS containing 20% Matrigel) into the right flank subcutaneously. Two weeks after cell injection, mice were randomly allocated to two groups (n = 5) and fed either control chow or chow containing 200 mg/kg doxycycline (Sigma-Aldrich), respectively. In addition, to determine whether CARD11 silencing could have an effect on tumor growth, we screened UOK111 and Caki cell lines for tumorigenicity and observed that UOK111 was non-tumorigenic; thus, we used Caki cells for *in vivo* tumor growth experiments. We established the Caki tumor model by injecting Caki cells (5 million cells/mouse in 100 μL of HBSS containing 20% Matrigel) into the right flank of mice subcutaneously. After 9 days, tumor establishment was checked and the mice were randomized and divided into 2 groups and treated with either control siRNA (n = 9) or CARD11 siRNA (n = 10). Mice were treated twice weekly starting on the tenth day after cell injection, with intravenous injections of either control siRNA or CARD11 siRNA incorporated into chitosan nanoparticles. Mice were observed twice weekly, and tumors were measured with hand held Vernier calipers. Tumor volumes were calculated as follows: volume = A x $B^2/2$ with ‘A’ being the greatest longitudinal diameter of the tumors, and ‘B’ being the greatest transverse diameter. At the end of the experiment, mice were sacrificed and tumors measured and weighed.

Tissue Microarray

Kidney cancer tumor microarray (TMA; CAT#: CT565866, OriGene Technologies Inc.) slides were deparaffinized in xylene and rehydrated with a gradient alcohol series followed by heat-mediated antigen retrieval (0.01 M sodium citrate buffer, pH 6.0). The slides were washed with PBS and blocked with 3% hydrogen peroxide for 10 min. TMAs were blocked for 30 min with 5% normal goat serum and then incubated with either rabbit polyclonal antibody against CARD11 (Abcam Cat# ab113409, RRID:AB_10861854; 1:200) or mouse monoclonal antibody against alpha smooth muscle actin (αSMA, clone 1A4) (Agilent Cat# M0851, RRID:AB_2223500; 1:300) at 4°C overnight in a humidified

chamber. The slides were later washed and incubated with HRP-conjugated anti-rabbit (for CARD11) and anti-mouse (for αSMA) secondary antibodies for 30 minutes at room temperature. Diaminobenzidine (DAB) was used for color development and the nuclei were counterstained with hematoxylin.

Reverse phase protein arrays (RPPA)

RPPA analysis was carried out by the UT MD Anderson Cancer Center RPPA core facility, as described previously (38). Briefly, H1975 cells were transfected with control siRNA or CARD11 siRNA for 72 h. Cell lysates were prepared in RIPA buffer (1% Triton X-100, 25 mM Tris, pH 7.4, 150 mM NaCl, 0.1% sodium dodecyl sulfate, 0.5% sodium deoxycholate) containing freshly added protease and phosphatase inhibitors. Protein concentrations were measured using a BCA assay kit (Pierce Biotechnology) and 40 μg of protein was used for RPPA analysis. Normalized RPPA data was processed through Ingenuity Pathway Analysis database (Ingenuity Pathway Analysis, RRID:SCR_008653).

Statistical Analysis

Statistics were performed using unpaired t-tests for comparisons between two groups and one-way ANOVA with Tukey's post-test for multiple comparisons or two-way ANOVA for more than two groups using Graphpad Prism (GraphPad Prism, RRID:SCR_002798). Statistical values were considered significant when $p < 0.05$ (*$p < 0.05$, **$p < 0.01$, ***$p < 0.001$).

Randomization and Blinding

No specific randomization procedure was employed in the *in vitro* experiments. In *in vivo* experiments, after tumor establishment animals were randomized (not blinded) and fed either control chow or dox-chow. At time of necropsy, all investigators were blinded to group allocation to assess outcome of the experiment.

RESULTS

CARD11 gene body DNA methylation is highly correlated with gene expression

To focus on genes in which gene body DNA methylation may play a role in cancer pathogenesis, we focused on the 260 genes listed in a recent study that catalogued *bona fide* tumor suppressors and oncogenes (39). These genes were cross-referenced with TCGA RNA-seq and DNA methylation array datasets, and an average correlation coefficient across the gene body was determined for 32 cancer types. Those genes with a correlation cutoff of > 0.5 in at least one tissue type were selected for further analysis (Fig. 1A). This yielded a list of 57 genes matching the criterion, with *CARD11* displaying this correlation in 19 out of 32 tumor tissues investigated. Based on this striking observation, the impact of *CARD11* was examined in further detail. This gene is well-known to be a driver of diffuse large B cell lymphoma (40); apart from squamous cell carcinoma (41), its role in other epithelial cancers has not been explored. Thus, the difference in expression of *CARD11* between 15 of the most common epithelial cancers and their corresponding normal tissues was evaluated using TCGA datasets. This revealed that *CARD11* is significantly overexpressed in 9 of the 15 tumor types, most substantially in kidney renal cell (KIRC) and lung adeno (LUAD)

carcinomas (Supplementary Table 2). Since *CARD11* has been considered a lymphocyte-specific gene, we also estimated immune cell infiltration levels in KIRC and LUAD samples. We used CIBERSORT analytical tool to estimate the abundance of 13 lymphocyte cell subpopulations in LUAD and KIRC TCGA cohorts using normalized RNA-seq data. We observed low to moderate correlation between *CARD11* expression with T-cell abundance in KIRC and LUAD cohorts from TCGA (Supplementary Table 3). The associations between *CARD11* expression and patient overall survival were then evaluated by tissue type. This revealed that high expression is correlated with shorter patient survival in KIRC (Fig. 1B). Moreover, higher gene body methylation of CARD11 is also correlated with poor patient survival in KIRC (Fig. 1C). To address whether increased levels of CARD11 protein levels were observed in patient tumor samples, a human KIRC tissue microarray was employed which showed high expression in 20 out of 33 tumors tissues analyzed. To confirm epithelial staining of CARD11, we performed IHC staining for CARD11 protein and a fibroblast marker (alpha smooth muscle actin, αSMA) on adjacent paraffin-embedded TMA slides. We observed epithelial-specific staining of CARD11 protein expression and there was no CARD11 expression noted in stromal fibroblasts, which stained positive for αSMA in the adjacent section (Fig 1D). These data indicate that *CARD11* expression is highly correlated with gene body methylation, that higher expression is observed in epithelial tumors, and that overexpression of *CARD11* may negatively impact survival of patients with KIRC.

CARD11 regulates the mTOR pathway and represses autophagy in epithelial cancers

Given the observed overexpression of *CARD11* across many epithelial cancer types, we next examined its functional and biological role in epithelial cancers. *CARD11* is considered an adaptor protein that links stimulation of the T and B cell receptors to activation of the NF-kB pathway. To understand the signaling pathways downstream of *CARD11*, an RPPA was performed on protein lysates from the H1975 lung adenocarcinoma cells in which *CARD11* was knocked down using siRNA. After running the RPPA data through the Ingenuity Pathway Analysis database, contrary to expectations, the NF-kB pathway was unchanged after *CARD11* knockdown. Instead, the mTOR pathway was the most impacted by knockdown of *CARD11*, with multiple components of the pathway exhibiting decreased activity or expression in this context (Fig. 2A). To confirm the regulation of mTOR by CARD11, the *CARD11* gene was knocked down by siRNA, and phosphorylation of the downstream mTOR signaling target S6 was determined as a measurement for mTOR activation. Additionally, among a panel of KIRC cell lines tested, the UOK111 cell line showed high expression of *CARD11*, and was selected for further analysis (Supplementary Fig. S1A). After *CARD11* knockdown, the amount of phosphorylated S6 decreased in both UOK111 and H1975 cell lines (Fig. 2B), validating the finding that the mTOR pathway is positively regulated by *CARD11*. Alternatively, *CARD11* was overexpressed in the *CARD11* negative cell line, A498. Upon overexpression, the amount of phosphorylated S6 was observed to increase, relative to the control (Supplementary Figure S1B). In addition, *CARD11* overexpression lead to increased colony formation in the *CARD11* negative A498 cells (Supplementary Fig. S1C). To substantiate our *in vitro* findings, we calculated the Spearman correlation coefficients between *CARD11* expression levels and mTOR pathway signature in KIRC TCGA-RNA-Seq data (Supplementary Table 4). We observed a strong positive correlation of *CARD11* expression with PI3K (PIK3G and PIK3CD), which is an

upstream activator of mTOR pathway. In addition, *CARD11* expression showed a negative correlation with CAB39L, which has been shown to inhibit the mTOR pathway (42). To further investigate correlation of *CARD11* expression on mTOR signaling signature, we ran GSEA analysis using KIRC TCGA RNA-Seq data and noticed enrichment of PI3K-AKT-mTOR pathway in patients with higher CARD11 expression (Supplementary Fig. S1E).

The mTOR pathway can affect a multitude of cellular processes, including transcription and autophagy (43). To test the biological consequences of *CARD11* silencing, UOK111 and H1975 cells were subjected to proliferation and cell cycle assays after *CARD11* knockdown. However, no significant change in either of these processes was observed. Similarly, there was no significant difference in apoptosis between control and *CARD11* siRNA groups (Supplementary Fig. S1D). Finally, the ability of the cells to establish single-cell colonies after *CARD11* knockdown was measured. Both UOK111 and H1975 cell lines showed significantly impaired colony-formation after *CARD11* knockdown (Fig. 2C).

mTOR activation is known to negatively regulate autophagy, and diminished autophagy is known to play a role in renal cell carcinoma pathogenesis (44). To test whether CARD11 can affect autophagy, the level of autophagy in UOK111 and H1975 cells after *CARD11* knockdown was determined using lipidated LC3 (LC3-II) as a marker. *CARD11* knockdown resulted in increased amounts of LC3-II in both cell lines tested (Fig. 2D and Supplementary Fig. S1F). Because an increase in LC3-II levels can be due to increased autophagosome assembly, or due to decreased fusion of the autophagosome with the lysosome, we next used bafilomycin A1 (autophagy inhibitor) to ascertain the cause of increased LC3-II levels. If fusion was compromised by *CARD11* knockdown, the addition of bafilomycin A1 should not result in any change in LC3-II levels. However, after adding bafilomycinA1, the levels of LC3-II increased substantially in *CARD11* siRNA transfected cells, indicating that knocking down of *CARD11* increased autophagy in both UOK111 and H1975 cells (Fig. 2D and Supplementary Fig. S1F). To further test this hypothesis, a GFP-RFP-tagged LC3 protein was expressed in H1975 cells, allowing for visualization of autophagic flux. The cells were then monitored using live-cell imaging by confocal microscopy after control siRNA or *CARD11* siRNA transfection. The cells in which CARD11 was knocked down exhibited an increased amount of RFP signal, indicating that these cells have greater autophagic flux relative to the control siRNA transfected cells (Fig. 2E–F).

CARD11 gene body CpG island DNA methylation regulates gene expression

As noted above, *CARD11* gene body methylation is strongly correlated with gene expression. To ascertain whether this modification is a driving factor in overexpression of *CARD11* in epithelial cancers, gene body methylation in tumor samples or corresponding normal tissues was compared, revealing an increase in gene body methylation of *CARD11* in KIRC and LUAD tumors, relative to normal tissues (Supplementary Table 5). To locate a specific region of DNA methylation that may impact *CARD11* expression, the gene body was examined using the Santa Cruz Genome Browser(45). This revealed that CpG island methylation within the gene body exhibited strong correlation with gene expression in KIRC and LUAD tumors (Fig. 3A, D and Supplementary Table 5). Treating UOK111 and H1975 cells with decitabine resulted in decreased *CARD11* expression; supporting the notion that

methylation increases its expression (Fig. 3B, C). The change in methylation between normal kidney tissue and renal cell carcinoma in TCGA samples was then evaluated and a significant increase in methylation in renal cell carcinoma was observed in each of the five sites interrogated in this region (Fig. 3D).

To determine whether methylation of the gene body CpG island could regulate expression of *CARD11*, site specific demethylation of a CpG island was achieved using a modified cas9 system, in which the catalytic portion of the DNA demethylating enzyme *TET1* was fused with a nickase-dead version of the *CAS9* gene. Guide RNAs were then designed to target this fusion protein to the CARD11 gene body CpG island, inducing an approximate 5% decrease in methylation at this region by Pyrosequencing (Fig. 3E). This was further confirmed by methylation analysis by PCR and after sgRNA mediated demethylation, the expression of *CARD11* was observed to be significantly decreased (Fig. 3F, G). A potential mediator of site-specific methylation is lnc-RNAs, with natural antisense transcripts (NATs) often involved in controlling the DNA methylation status of its transcriptional locus (46). *CARD11* has a natural antisense transcript located within the gene body, approximately 20,000 base pairs upstream of the CpG island (Supplementary Fig. S2A); therefore, it was hypothesized that the *CARD11* Natural Antisense Transcript (*CARD11*-NAT) is involved in methylation of the *CARD11* gene body. *CARD11*-NAT expression is highly correlated with *CARD11* expression (Supplementary Fig. S2B), and higher expression of *CARD11*-NAT is associated with higher *CARD11* gene body methylation in both KIRC and LUAD. In addition, *CARD11*-NAT is significantly overexpressed in these two tumor types, relative to normal tissues (Supplementary Fig. S2C). However, upon overexpression of *CARD11*-NAT in the context of *CARD11* CpG island demethylation, no increase in *CARD11* expression was observed (Supplementary Fig. S2D).

CARD11 expression regulates renal cell carcinoma growth

To evaluate the effect of increased *CARD11* expression on tumor growth, we engineered A498 cells to express doxycycline (dox)-inducible CARD11 protein. Doxycycline treatment induced a time dependent increase in CARD11 expression (Fig. 4A). In addition, dox-induced CARD11 expression lead to mTOR activation, evidenced by increased S6 phosphorylation, which was suppressed in the presence of mTOR inhibitor, rapamycin (Fig. 4B). Further, to examine the requirement of CARD11 expression for tumor growth, Dox-inducible CARD11 expressing A498 cells were injected into immunocompromised mice and expression of CARD11 was induced by feeding mice with Dox-chow. Confirming our *in vitro* observations doxycycline treated xenografts displayed a significant increase in tumor growth (Fig. 4C) and tumor weight (Fig. 4D). In addition, to knockdown *CARD11* expression in Caki tumors, we delivered *CARD11* siRNA using intravenous chitosan nanoparticles twice weekly. There was a significant decrease in tumor growth (Fig. 4E) and tumor weight (Fig. 4F) upon CARD11 knockdown in the Caki tumor model.

DISCUSSION

The main findings from our work include: 1) aberrant expression of *CARD11* can promote cancer pathogenesis through changes to mTOR signaling and autophagy, and 2)

CARD11 gene body methylation results in increased gene expression. This study expands our understanding of the creative means by which tumor cells activate genes otherwise unexpressed in their tissue of origin, and to co-opt downstream signaling pathways that serve to propel malignant biology forward. In the case of *CARD11*, this lymphocyte-specific gene canonically links the T- and B-cell receptors to the NF-kB pathway, thereby mediating lymphocyte activation upon antigen stimulation. Surprisingly, knockdown of *CARD11* did not affect the NF-kB pathway, instead conveying its effects primarily through the mTOR axis. CARD11 has been shown previously to be involved in mTOR activation in T cells (47), but to our knowledge, this is the first such observation in epithelial cells. In T-cells, CARD11 has been shown to regulate mTOR signaling through proteolytic activity of MALT1 (47) and the uptake of glutamine through ASCT2 (48).

While localized renal cell carcinoma can be eliminated through procedures such as resection of the kidney or heat/cold ablation therapy, approximately one third of patients with clear cell renal cell carcinoma develop metastasis (49). Current clinical trials combining mTOR inhibitors with MAPK inhibitors have been limited by toxicity (50); therefore, new, less toxic approaches in targeting the mTOR pathway are needed. Moreover, targeting *CARD11* gene body methylation may provide a highly selective means by which *CARD11* expression, and downstream mTOR signaling, may be suppressed. However, the prevalence of *CARD11* gene body methylation in T and B cells, and how demethylation affects the function of these cells, requires further investigation before targeting this region for clinical applications.

In addition to further supporting the finding that tumor cells can utilize non-canonical pathways, this analysis also reveals how tumor cells employ non-canonical mechanisms to induce aberrant expression of genes that are otherwise silenced by their tissue of origin. Previous studies have uncovered various means by which this process is undertaken. These include promoter demethylation, upregulation of transcription factors, changes to chromatin architecture, and downregulation of microRNAs, among many others. Here, we have provided further evidence that gene body DNA methylation is an alternative mechanism by which tumor cells can alter their transcriptional profile during tumorigenesis and tumor progression. This serves to reiterate the importance of examining gene body DNA methylation as a means of fully understanding transcriptional regulation, and that targeting this type of epigenetic modification is a newly emerging route to modulate aberrant gene expression.

The past 20 years have seen gene regulation by RNAs becoming more prominent and expansive. Lnc-RNAs can induce changes to chromatin, recruit transcription factors, or bind mRNAs. Importantly, they are also known to modulate DNA methylation by associating with DNMT1, DNMT3A & B, or GADD45A/TDG, among others. Despite these unique properties, the vast majority of the antisense RNAome has not been fully studied. A certain portion of these antisense RNAs may not serve a function at all, and can be discarded as transcriptional noise, but this study highlights the need to catalog the thousands of antisense RNAs that exist, and how they are involved in normal and abnormal cellular processes. As systemic siRNA therapies become more accepted in the clinic, antisense RNAs make promising candidates for a new frontier of targets in cancer. However, in this study, we determined that the *CARD11-NAT* does not regulate *CARD11*. Despite this, we

have concluded that these two transcripts are co-regulated by the gene body CpG island. Considering *CARD11-NAT* is spliced and highly overexpressed in multiple cancer types, it could be functionally relevant both for normal cellular processes as well as in cancer. On the other hand, its increased expression in cancer may simply be a byproduct of increased *CARD11* expression. The role this NAT plays in cellular biology must be further explored.

In conclusion, these data have revealed that *CARD11* is upregulated in certain epithelial cancers, and its overexpression is strongly associated with decreased patient survival in kidney renal cell carcinoma. CARD11 can activate the mTOR pathway in the context of epithelial cancer, while not impacting the canonical NF-kB pathway. The expression of *CARD11* is regulated by methylation of the CpG island within the gene body, which increases expression. Therefore, this study emphasizes the importance of considering how methylation can increase expression of oncogenes, and provides novel insight into how oncogenes are activated during tumorigenesis and tumor progression.

Supplementary Material

Refer to Web version on PubMed Central for supplementary material.

ACKNOWLEDGEMENTS

We thank Dr. Marcos Estecio and the MDACC Epigenomics Profiling Core for performing the methylation assays. Cells were analyzed by the MD Anderson Flow Cytometry and Cellular Imaging Core Facility (this facility is funded by NCI Cancer Center Support Grant P30 CA16672). This work was supported, in part by grants to AKS, by the NIH (P50 CA217685, P50 CA098258, P50 CA098250 and R35 CA209904), Marsha Rivkin Center for Ovarian Cancer, the National Comprehensive Cancer Network, American Cancer Society Research Professor Award, Judy's Mission, and the Frank McGraw Memorial Chair in Cancer Research. AKS was also supported by the Blanton-Davis Ovarian Cancer Research Program. We would like to acknowledge Don Norwood (Department of Scientific Publications at MD Anderson) for editing this manuscript.

Grant Support:

This work was supported, in part by grants to AKS, by the NIH (P50 CA217685, P50 CA098258, P50 CA098250 and R35 CA209904), Marsha Rivkin Center for Ovarian Cancer, the National Comprehensive Cancer Network, American Cancer Society Research Professor Award, Judy's Mission, and the Frank McGraw Memorial Chair in Cancer Research. This work was also supported by the NIH/NCI under award number P30CA016672.

REFERENCES

1. Edwards JR, Yarychkivska O, Boulard M, Bestor TH. DNA methylation and DNA methyltransferases. Epigenetics & Chromatin. 2017;10(1):23. [PubMed: 28503201]
2. Smith ZD, Meissner A. DNA methylation: roles in mammalian development. Nature Reviews Genetics. 2013;14:204.
3. Suzuki MM, Bird A. DNA methylation landscapes: provocative insights from epigenomics. Nature Reviews Genetics. 2008;9:465.
4. Weber M, Hellmann I, Stadler MB, Ramos L, Pääbo S, Rebhan M, et al. Distribution, silencing potential and evolutionary impact of promoter DNA methylation in the human genome. Nature Genetics. 2007;39:457. [PubMed: 17334365]
5. Wu H, Coskun V, Tao J, Xie W, Ge W, Yoshikawa K, et al. Dnmt3a-dependent nonpromoter DNA methylation facilitates transcription of neurogenic genes. Science. 2010;329(5990):444–8. [PubMed: 20651149]
6. Niles KM, Chan D, La Salle S, Oakes CC, Trasler JM. Critical Period of Nonpromoter DNA Methylation Acquisition during Prenatal Male Germ Cell Development. PLOS ONE. 2011;6(9):e24156. [PubMed: 21949694]

7. Flores KB, Amdam GV. Deciphering a methylome: what can we read into patterns of DNA methylation? The Journal of Experimental Biology. 2011;214(19):3155–63. [PubMed: 21900463]
8. Flintoft L Looking beyond promoters. Nature Reviews Genetics. 2010;11:596.
9. Irvine RA, Lin IG, Hsieh C-L. DNA Methylation Has a Local Effect on Transcription and Histone Acetylation. Molecular and Cellular Biology. 2002;22(19):6689–96. [PubMed: 12215526]
10. King AD, Huang K, Rubbi L, Liu S, Wang C-Y, Wang Y, et al. Reversible Regulation of Promoter and Enhancer Histone Landscape by DNA Methylation in Mouse Embryonic Stem Cells. Cell reports. 2016;17(1):289–302. [PubMed: 27681438]
11. Heyn H, Vidal E, Ferreira HJ, Vizoso M, Sayols S, Gomez A, et al. Epigenomic analysis detects aberrant super-enhancer DNA methylation in human cancer. Genome Biology. 2016;17(1):11. [PubMed: 26813288]
12. Kulis M, Queiros AC, Beekman R, Martin-Subero JI. Intragenic DNA methylation in transcriptional regulation, normal differentiation and cancer. Biochim Biophys Acta. 2013;1829(11):1161–74. [PubMed: 23938249]
13. Wu H, Coskun V, Tao J, Xie W, Ge W, Yoshikawa K, et al. Dnmt3a-Dependent Nonpromoter DNA Methylation Facilitates Transcription of Neurogenic Genes. Science (New York, NY). 2010;329(5990):444–8.
14. Murgatroyd C, Patchev AV, Wu Y, Micale V, Bockmühl Y, Fischer D, et al. Dynamic DNA methylation programs persistent adverse effects of early-life stress. Nature Neuroscience. 2009;12:1559. [PubMed: 19898468]
15. Jones PA. Functions of DNA methylation: islands, start sites, gene bodies and beyond. Nat Rev Genet. 2012;13(7):484–92. [PubMed: 22641018]
16. Robertson KD. DNA methylation and human disease. Nature Reviews Genetics. 2005;6:597.
17. Conerly M, Grady WM. Insights into the role of DNA methylation in disease through the use of mouse models. Disease Models & Mechanisms. 2010;3(5–6):290–7. [PubMed: 20427558]
18. Gopalakrishnan S, Emburgh BOV, Robertson KD. DNA methylation in development and human disease. Mutation research. 2008;647(1–2):30–8. [PubMed: 18778722]
19. Miranda-Morales E, Meier K, Sandoval-Carrillo A, Salas-Pacheco J, Vázquez-Cárdenas P, Arias-Carrión O. Implications of DNA Methylation in Parkinson's Disease. Frontiers in Molecular Neuroscience. 2017;10(225).
20. Lu H, Liu X, Deng Y, Qing H. DNA methylation, a hand behind neurodegenerative diseases. Frontiers in Aging Neuroscience. 2013;5(85).
21. Klein H-U, De Jager PL. Uncovering the Role of the Methylome in Dementia and Neurodegeneration. Trends in Molecular Medicine.22(8):687–700. [PubMed: 27423266]
22. Lund G, Andersson L, Lauria M, Lindholm M, Fraga MF, Villar-Garea A, et al. DNA methylation polymorphisms precede any histological sign of atherosclerosis in mice lacking apolipoprotein E. J Biol Chem. 2004;279(28):29147–54. [PubMed: 15131116]
23. Movassagh M, Choy MK, Goddard M, Bennett MR, Down TA, Foo RS. Differential DNA methylation correlates with differential expression of angiogenic factors in human heart failure. PLoS One. 2010;5(1):e8564. [PubMed: 20084101]
24. Kim M, Long TI, Arakawa K, Wang R, Yu MC, Laird PW. DNA methylation as a biomarker for cardiovascular disease risk. PLoS One. 2010;5(3):e9692. [PubMed: 20300621]
25. Richardson B DNA methylation and autoimmune disease. Clin Immunol. 2003;109(1):72–9. [PubMed: 14585278]
26. Yung RL, Quddus J, Chrisp CE, Johnson KJ, Richardson BC. Mechanisms of drug-induced lupus: I. Cloned Th2 cells modified with DNA methylation inhibitors in vitro cause autoimmunity in vivo. Journal of Immunology. 1995;154(6):3025–35.
27. Richardson B Effect of an inhibitor of DNA methylation on T cells. II. 5-Azacytidine induces self-reactivity in antigen-specific T4+ cells. Hum Immunol. 1986;17(4):456–70. [PubMed: 2432050]
28. Kulis M, Esteller M. DNA methylation and cancer. Adv Genet. 2010;70:27–56. [PubMed: 20920744]
29. Ehrlich M DNA methylation in cancer: too much, but also too little. Oncogene. 2002;21:5400. [PubMed: 12154403]

30. Tokarz P, Pawlowska E, Bialkowska-Warzecha J, Blasiak J. The significance of DNA methylation profile in metastasis-related genes for the progression of colorectal cancer. Cell Mol Biol (Noisy-le-grand). 2017;63(2):79–87.
31. Abu shahin F, Green A, Wang L, Zhang X, Yang B. DNA methylation profiling associates with chemoresistance and early recurrence in papillary serous carcinoma of the ovary. Cancer Research. 2007;67(9 Supplement):1113–. [PubMed: 17283145]
32. Zhang MW, Fujiwara K, Che X, Zheng S, Zheng L. DNA methylation in the tumor microenvironment. J Zhejiang Univ Sci B. 2017;18(5):365–72. [PubMed: 28471108]
33. Yang X, Han H, De Carvalho DD, Lay FD, Jones PA, Liang G. Gene Body Methylation can alter Gene Expression and is a Therapeutic Target in Cancer. Cancer cell. 2014;26(4):577–90. [PubMed: 25263941]
34. Chen K, Zhang J, Guo Z, Ma Q, Xu Z, Zhou Y, et al. Loss of 5-hydroxymethylcytosine is linked to gene body hypermethylation in kidney cancer. Cell Research. 2015;26:103. [PubMed: 26680004]
35. Chodavarapu RK, Feng S, Bernatavichute YV, Chen PY, Stroud H, Yu Y, et al. Relationship between nucleosome positioning and DNA methylation. Nature. 2010;466(7304):388–92. [PubMed: 20512117]
36. McGuire MH, Herbrich SM, Dasari SK, Wu SY, Wang Y, Rupaimoole R, et al. Pan-cancer genomic analysis links 3'UTR DNA methylation with increased gene expression in T cells. EBioMedicine. 2019;43:127–37. [PubMed: 31056473]
37. Estecio MR, Yan PS, Ibrahim AE, Tellez CS, Shen L, Huang TH, et al. High-throughput methylation profiling by MCA coupled to CpG island microarray. Genome Res. 2007;17(10):1529–36. [PubMed: 17785535]
38. Tibes R, Qiu Y, Lu Y, Hennessy B, Andreeff M, Mills GB, et al. Reverse phase protein array: validation of a novel proteomic technology and utility for analysis of primary leukemia specimens and hematopoietic stem cells. Mol Cancer Ther. 2006;5(10):2512–21. [PubMed: 17041095]
39. Lawrence MS, Stojanov P, Mermel CH, Robinson JT, Garraway LA, Golub TR, et al. Discovery and saturation analysis of cancer genes across 21 tumour types. Nature. 2014;505:495. [PubMed: 24390350]
40. Lenz G, Davis RE, Ngo VN, Lam L, George TC, Wright GW, et al. Oncogenic CARD11 mutations in human diffuse large B cell lymphoma. Science. 2008;319(5870):1676–9. [PubMed: 18323416]
41. Watt SA, Purdie KJ, den Breems NY, Dimon M, Arron ST, McHugh AT, et al. Novel CARD11 Mutations in Human Cutaneous Squamous Cell Carcinoma Lead to Aberrant NF-kappaB Regulation. Am J Pathol. 2015;185(9):2354–63. [PubMed: 26212909]
42. Pulito C, Mori F, Sacconi A, Goeman F, Ferraiuolo M, Pasanisi P, et al. Metformin-induced ablation of microRNA 21–5p releases Sestrin-1 and CAB39L antitumoral activities. Cell Discov. 2017;3:17022. [PubMed: 28698800]
43. Laplante M, Sabatini DM. mTOR signaling in growth control and disease. Cell. 2012;149(2):274–93. [PubMed: 22500797]
44. Liu X-D, Zhu H, DePavia A, Jonasch E. Dysregulation of HIF2α and autophagy in renal cell carcinoma. Molecular & Cellular Oncology. 2015;2(2):e965643. [PubMed: 27308417]
45. Kent WJ, Sugnet CW, Furey TS, Roskin KM, Pringle TH, Zahler AM, et al. The human genome browser at UCSC. Genome Res. 2002;12(6):996–1006. [PubMed: 12045153]
46. Zhao Y, Sun H, Wang H. Long noncoding RNAs in DNA methylation: new players stepping into the old game. Cell & Bioscience. 2016;6:45. [PubMed: 27408682]
47. Hamilton KS, Phong B, Corey C, Cheng J, Gorentla B, Zhong X, et al. T cell receptor-dependent activation of mTOR signaling in T cells is mediated by Carma1 and MALT1, but not Bcl10. Sci Signal. 2014;7(329):ra55. [PubMed: 24917592]
48. Nakaya M, Xiao Y, Zhou X, Chang JH, Chang M, Cheng X, et al. Inflammatory T cell responses rely on amino acid transporter ASCT2 facilitation of glutamine uptake and mTORC1 kinase activation. Immunity. 2014;40(5):692–705. [PubMed: 24792914]
49. Frank I, Blute ML, Cheville JC, Lohse CM, Weaver AL, Zincke H. An outcome prediction model for patients with clear cell renal cell carcinoma treated with radical nephrectomy based on tumor stage, size, grade and necrosis: the SSIGN score. J Urol. 2002;168(6):2395–400. [PubMed: 12441925]

50. Patel PH, Senico PL, Curiel RE, Motzer RJ. Phase I study combining treatment with temsirolimus and sunitinib malate in patients with advanced renal cell carcinoma. Clin Genitourin Cancer. 2009;7(1):24–7. [PubMed: 19213664]

IMPLICATIONS

Our study describes a novel regulatory role of gene body DNA methylation-dependent CARD11 expression on mTOR signaling and its impact on tumor progression.

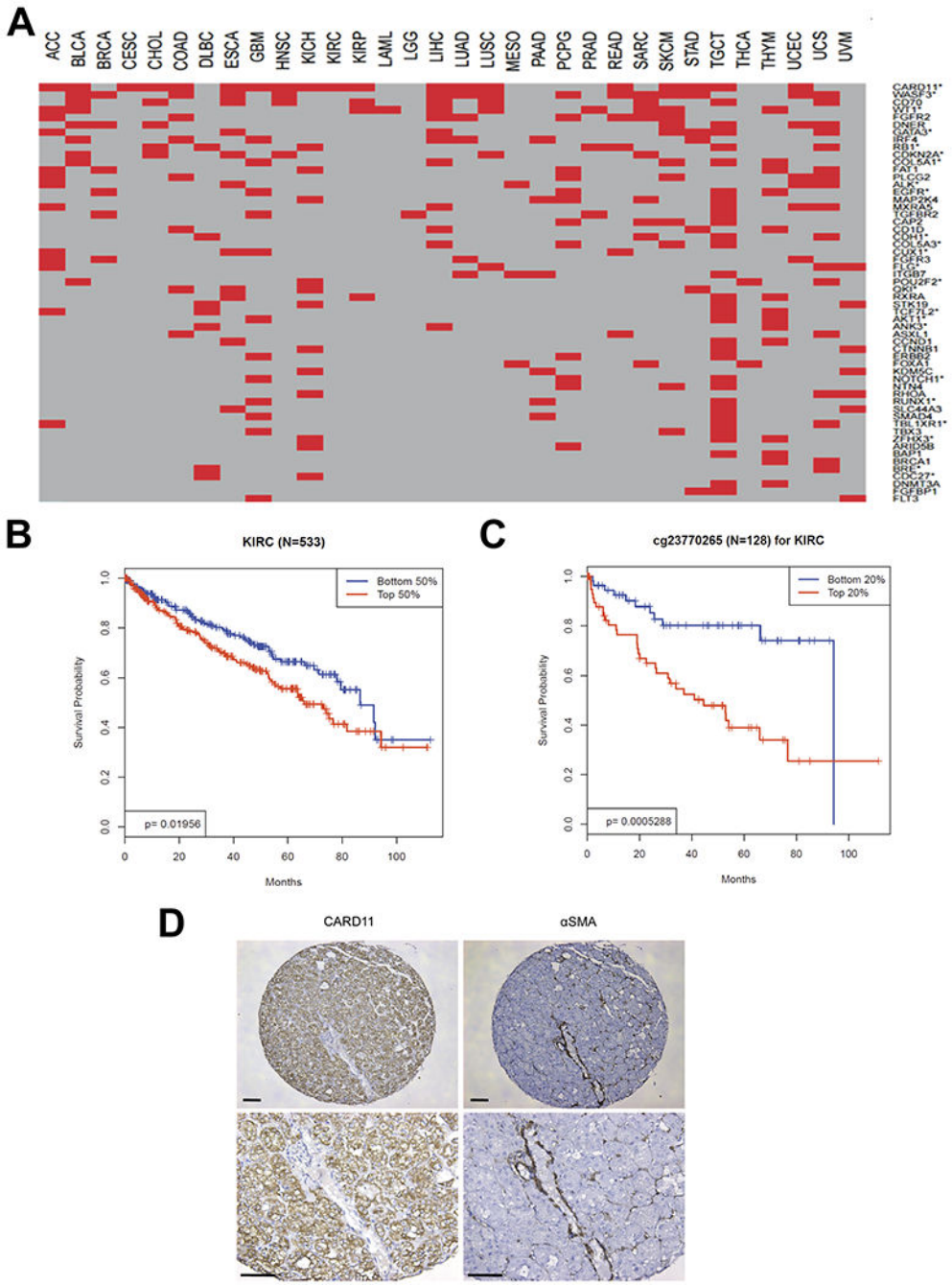

Figure 1: *CARD11* gene body methylation in cancer.

(A) Heat map of all high confidence cancer-related genes with a correlation coefficient of >0.5 between gene body methylation and gene expression are shaded red across 32 cancer types. (B) Association between *CARD11* expression and overall survival in kidney renal cell carcinoma patients. (C) Association between *CARD11* gene body methylation and overall survival in kidney renal cell carcinoma patients. (D) CARD11 immunohistochemical staining in representative kidney renal cell carcinoma sample showing high expression in epithelial cells. (Scale bar = 100 μm)

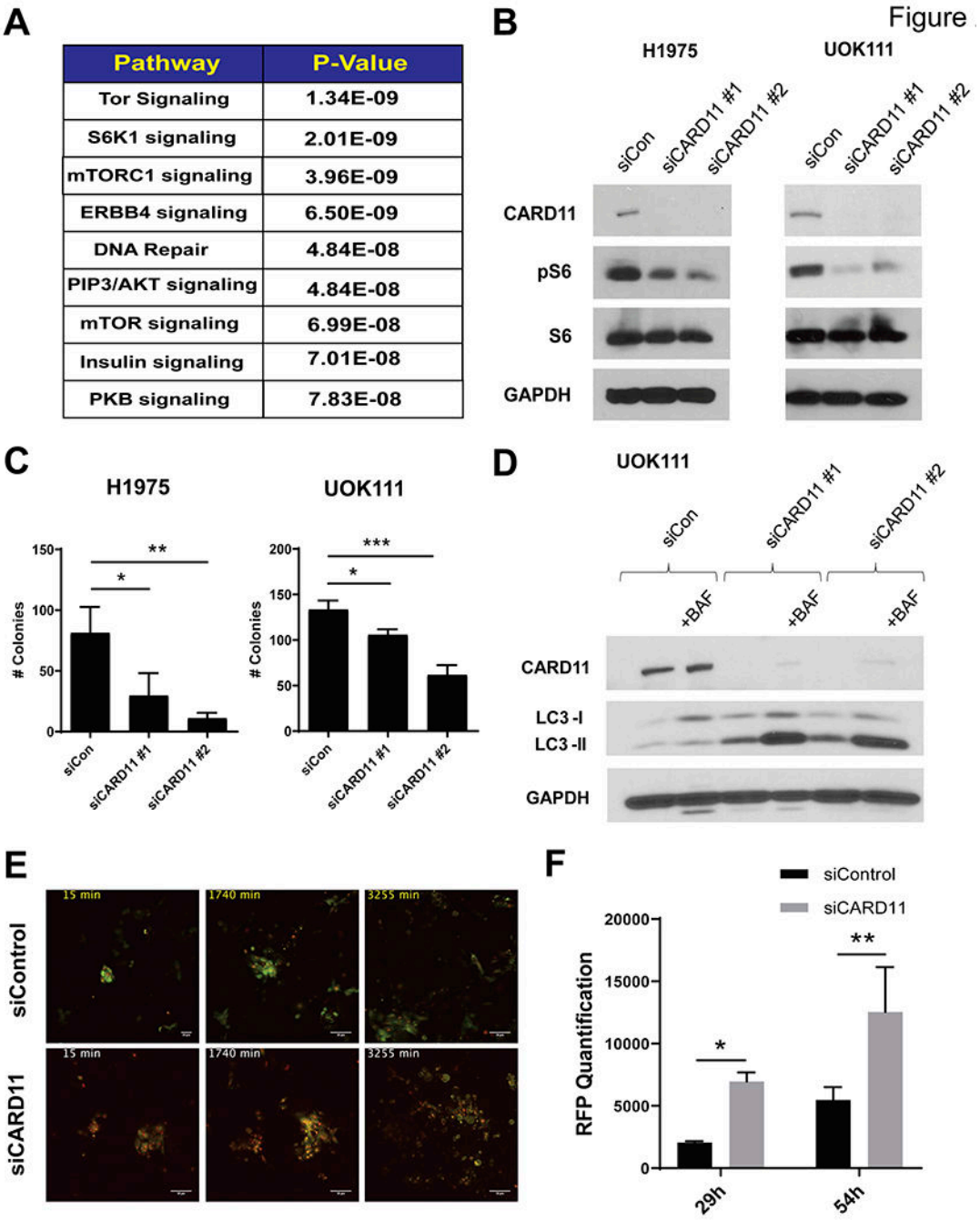

Figure 2: *CARD11* regulates mTOR signaling and autophagy.

(A) Pathways significantly downregulated upon CARD11 knockdown in H1975 cells. (B) CARD11 knockdown inhibits S6 phosphorylation in H1975 and UOK111 cells. (C) Impact of CARD11 knockdown on colony formation. (D) Effect of CARD11 knockdown on LC3 lipidation (BAF = bafilomycin A1). (E) Impact of CARD11 knockdown on autophagic flux in GFP-RFP-LC3 expressing cells. (F) Effect of CARD11 knockdown on autophagic flux quantification. Statistics were performed using unpaired t-tests for comparisons between two groups and one-way ANOVA with Tukey's post-test for multiple comparisons or Two-way

ANOVA for more than 2 groups. Statistical values were considered significant when $p < 0.05$ (*$p < 0.05$, **$p < 0.01$, ***$p < 0.001$). (Scale bar = 20 μm)

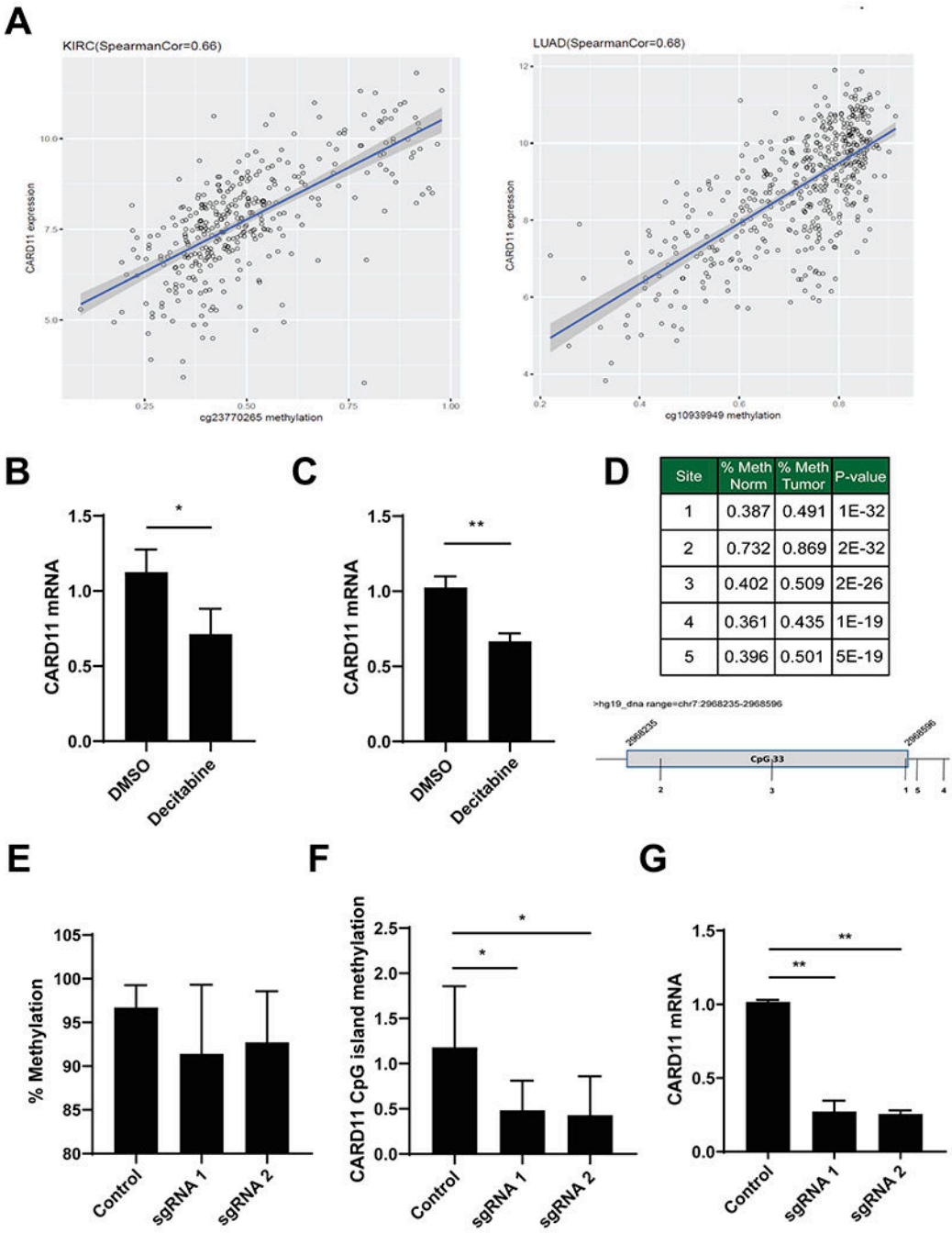

Site	% Meth Norm	% Meth Tumor	P-value
1	0.387	0.491	1E-32
2	0.732	0.869	2E-32
3	0.402	0.509	2E-26
4	0.361	0.435	1E-19
5	0.396	0.501	5E-19

Figure 3: *CARD11* gene body methylation regulates its expression.

(A) Correlation of *CARD11* gene body DNA methylation and gene expression in KIRC and LUAD. (B-C) Effect of DNA methylation inhibition on *CARD11* expression. (D) Change in methylation between normal kidney tissue and renal cell carcinoma in *CARD11* gene body CpG island associated methylation sites. (E) *CARD11* gene body methylation analysis by pyrosequencing. (F) *CARD11* gene body methylation analysis by PCR. (G) Effect of gene body demethylation on *CARD11* gene expression. Statistics were performed using unpaired t-tests for comparisons between two groups and one-way ANOVA with Tukey's post-test for

multiple comparisons for more than 2 groups. Statistical values were considered significant when $p < 0.05$ (*$p < 0.05$, **$p < 0.01$, ***$p < 0.001$).

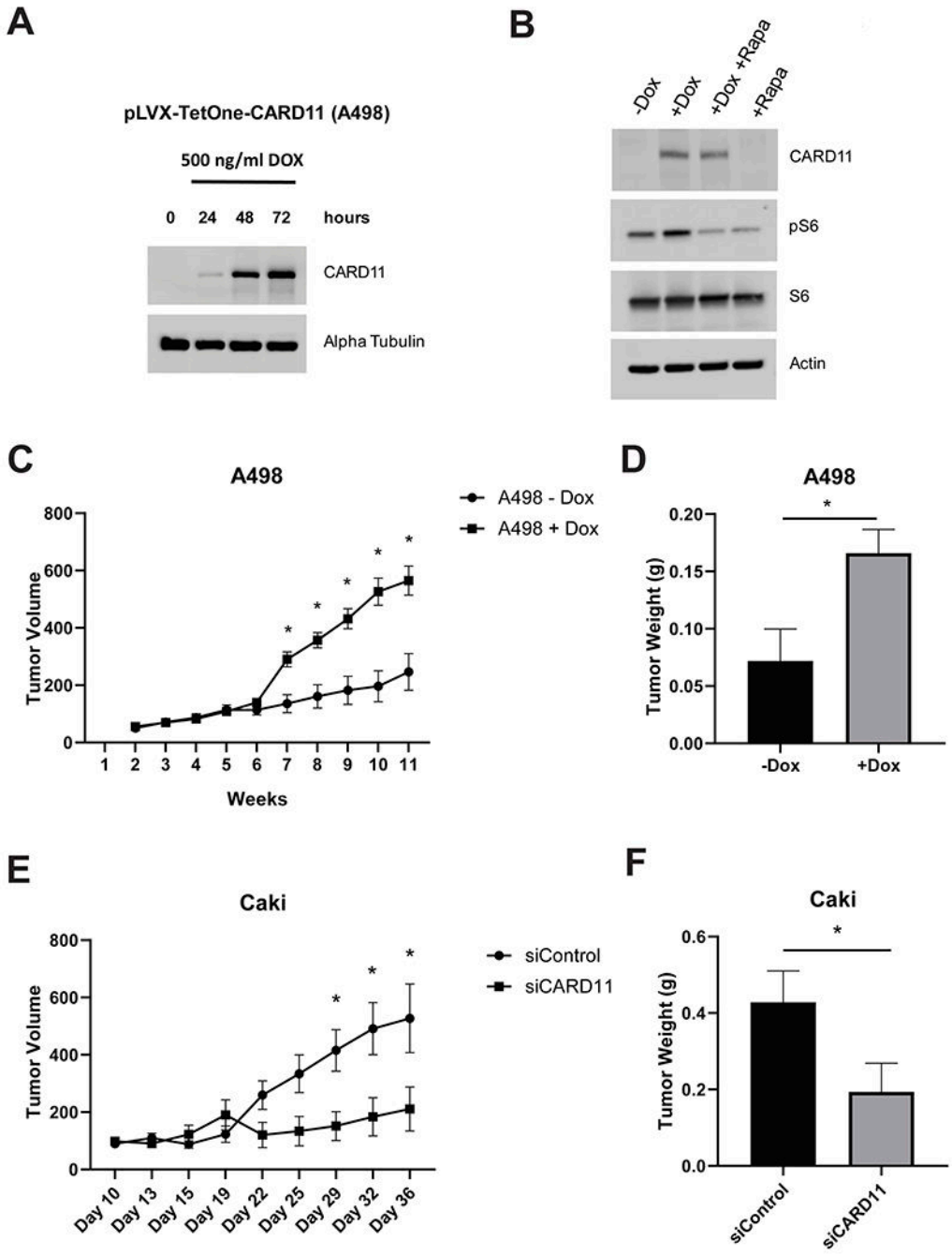

Figure 4: *CARD11* overexpression induces tumor growth.

(A) Doxycycline-induced CARD11 overexpression in A498 cells. (B) Effect of mTOR inhibition on CARD11 induced S6 phosphorylation. (C-D) Tumor volume and tumor weight of doxycycline-induced subcutaneous A498 tumor model. (E-F) Tumor volume and tumor weight of subcutaneous Caki tumor model. Statistics were performed using unpaired t-tests for comparisons between two group or two-way ANOVA for more than 2 groups. Statistical values were considered significant when $p < 0.05$ (*$p < 0.05$).